Biomacromolecules

pubs.acs.org/Biomac

Article

Comparison of Physicochemical Properties of Native Mucus and Reconstituted Mucin Gels

Caroline E. Wagner,*,○ Miri Krupkin,○ Kathryn B. Smith-Dupont,○ Chloe M. Wu, Nicole A. Bustos, Jacob Witten, and Katharina Ribbeck*

Cite This: *Biomacromolecules* 2023, 24, 628−639

Read Online

ACCESS | Metrics & More | Article Recommendations

ABSTRACT: Simulating native mucus with model systems such as gels made from reconstituted mucin or commercially available polymers presents experimental advantages including greater sample availability and reduced inter- and intradonor heterogeneity. Understanding whether these gels reproduce the complex physical and biochemical properties of native mucus at multiple length scales is critical to building relevant experimental models, but few systematic comparisons have been reported. Here, we compared bulk mechanical properties, microstructure, and biochemical responses of mucus from different niches, reconstituted mucin gels (with similar pH and polymer concentrations as native tissues), and commonly used commercially available polymers. To evaluate gel properties across these length scales, we used small-amplitude oscillatory shear, single-particle tracking, and microaffinity chromatography with small analytes. With the exception of human saliva, the mechanical response of mucin gels was qualitatively similar to that of native mucus. The transport behavior of charged peptides through native mucus gels was qualitatively reproduced in gels composed of corresponding isolated mucins. Compared to native mucus, we observed substantial differences in the physicochemical properties of gels reconstituted from commercially available mucins and the substitute carboxymethylcellulose, which is currently used in artificial tear and saliva treatments. Our study highlights the importance of selecting a mucus model system guided by the length scale relevant to the scientific investigation or disease application.

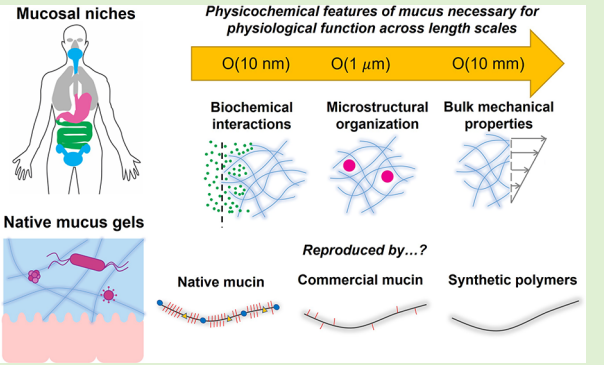

INTRODUCTION

Mucus provides a protective layer against mechanical, chemical, and microbial insults[1−4] and operates as a selective barrier capable of excluding foreign or harmful molecules on the basis of both size and biochemical properties[5−7] while permitting the passage of desirable agents.[4,8] The protective functions of mucus rely on a set of physical and chemical properties that span length scales. At the macroscale, bulk viscoelastic properties govern mucus' ability to lubricate and clear away harmful substances via processes such as coughing and mucociliary clearance (MCC). On the other hand, microstructural organization and biochemical patterns can impact the selective transport and adhesive properties of mucus in the context of passage of small molecules such as viruses and drug-delivery vehicles. Changes in these important mucosal properties are associated with various physiological conditions, including cystic fibrosis (CF)[5,9,10] and preterm birth.[11,12] Thus, studying mucus properties across a range of length scales is critical to understand how physicochemical parameters contribute to mucus function and dysfunction. Physiologically relevant substitute mucus systems can enable such investigative work and may have applications such as the treatment of diseases characterized by dry mucosal surfaces.

The native structure and function of mucus relevant to these diverse physiological functions are best retained in harvested whole mucus samples. However, the high degree of heterogeneity within tissue samples from a given donor (human or animal), as well as between donors, may lower the reproducibility and interpretability of the tests performed.[13−15] In addition, these tissues are typically difficult to source and limited in quantity.[13,16] For these reasons, substitute materials have been used in place of native mucus in several studies. For instance, synthetic polymers such as methylcellulose have been used to simulate the mechanical properties of mucus, yet biochemically, this polymer does not interact with microbes or other molecules in a way comparable

Received: August 16, 2022
Revised: December 1, 2022
Published: February 2, 2023

https://doi.org/10.1021/acs.biomac.2c01016
Biomacromolecules 2023, 24, 628−639

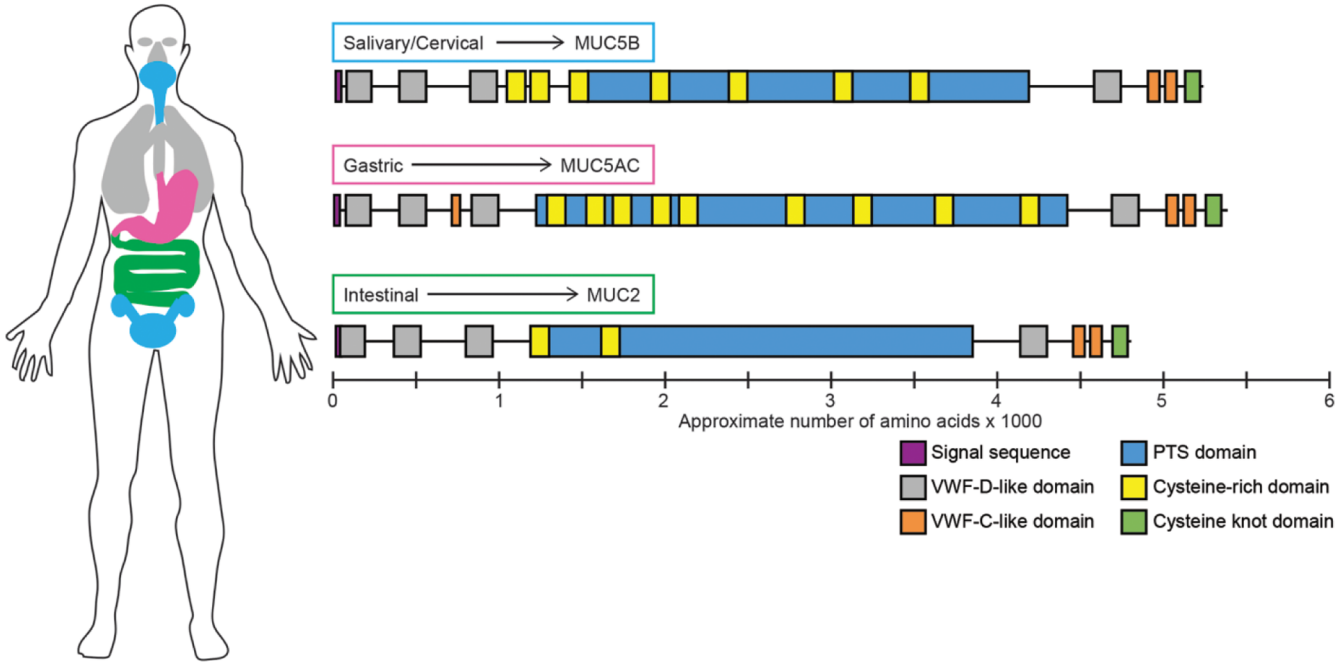

Figure 1. Domain structures of major gel-forming mucins expressed in salivary, cervical, gastric, and intestinal mucus reveal distinct structural differences. Note that in this work, MUC5AC and MUC2 are obtained from porcine sources that are analogous to human tissues, as indicated. The MUC5B used in this study was obtained from human sublingual gland expressions. All three gel-forming mucins contain Von Willibrand Factor (VWF), cysteine-rich, C-terminal cysteine knot, and heavily *O*-glycosylated proline/serine/threonine (PTS)-rich domains that are common to all gel-forming mucins in the MUC family. Domain locations and total protein lengths are approximated from Dekker et al.[21] This schematic highlights the mucosal niches we focus on in this study, but other tissues including the lungs also contain mucins.

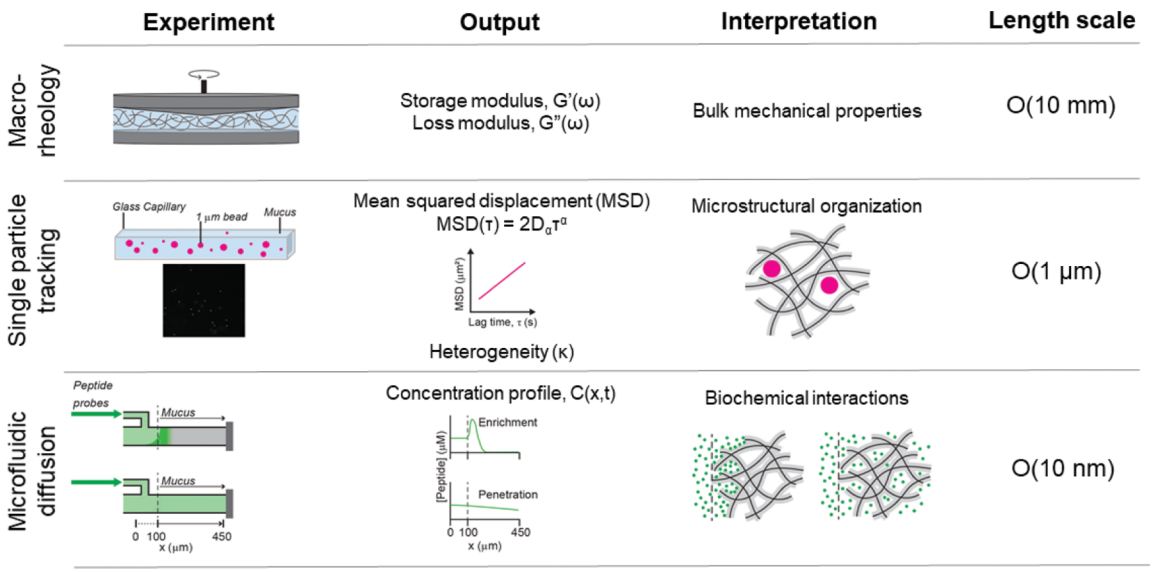

Figure 2. Schematic of the experimental approaches and readouts used to investigate the physicochemical properties of mucus and mucin gels at the millimeter, micrometer, and nanometer scales. Macrorheology, and SAOS in particular, was used to explore the bulk mechanical response of various gels by interpreting the frequency-dependent storage (G') and loss (G'') moduli. SPT was used to explore the microstructures of the various gels by analyzing the heterogeneity of the particle trajectories and their ensemble-average MSD. A microfluidic diffusion assay was used to explore the biochemical composition of the various gels by analyzing the diffusion profiles of small, positively and negatively charged peptide probes. The microfluidic diffusion schematic is adapted with permission from Smith-Dupont et al.,[12] originally published in *Scientific Reports* under a Creative Commons Attribution 4.0 International license.

to native mucus.[17] Another frequently used substitute is a gel reconstituted from purified native mucins.[1] Although these gels do not feature many of the other macromolecular components (e.g., lipids, antibodies) of mucus, reconstituted mucin gels have been shown to recapitulate important mechanical properties of mucus in specific cases.[1] Ultimately, the applicability of a mucus model system may be highly dependent on the length scale relevant to the physiological process being interrogated. Despite this, a systematic comparison of model mucus gels and native mucus across multiple length scales and in different mucosal niches is lacking.

https://doi.org/10.1021/acs.biomac.2c01016
Biomacromolecules 2023, 24, 628−639

Native mucus is composed primarily of water (~95%); it also contains lipids, salts, and proteins involved in defense such as immunoglobulins.[4] The primary structural component of mucus is the large glycoprotein mucin, which is composed of a protein backbone and primarily *O*-linked glycan structures arranged in a bottle brush-like fashion. These glycan structures account for ~80% of the molecular weight of mucin.[18] Within the mucin family, two important subgroups are frequently distinguished: (1) tethered, cell surface-associated mucins and (2) gel-forming, oligomeric mucins that exist as extensively polymerized, linear molecules and reside entirely outside of the epithelial cell layer.[19] The various mucosal surfaces of the body are composed of unique ratios of one or several types of these mucin molecules[19] and consequently possess specific mechanical and biochemical properties depending on their location in the body and intended physiological function.[20] Schematics of the domain structures of the three major gel-forming mucins, MUC2, MUC5AC, and MUC5B, along with the native mucosal tissues in which they are predominantly expressed, are shown in Figure 1.

In this investigation, we used three experimental platforms that separately highlight distinct physicochemical features of mucus gels over a range of length scales (Figure 2). We designed a systematic study to assess the degree to which reconstituted mucin gels, commercial mucins, and synthetic mucin-like polymers reproduce the properties of native mucus secretions. First, we performed small-amplitude oscillatory shear (SAOS) flow experiments to assess the macroscopic rheological response of the gels over length scales comparable to the size of the attached geometry (typically 8−60 mm). Next, we used single-particle tracking (SPT) to gain further insight into the microstructural organization of the gels over length scales comparable to the size of the probe particles (1 μm in diameter). Finally, we employed an assay that is mechanistically and conceptually similar to traditional affinity chromatography to probe the matrix behavior; in this assay, mucus represents the stationary phase and small analytes are used as probes to assess matrix interactions.

MATERIALS AND METHODS

Preparation of Carboxymethylcellulose (CMC) and Sigma Porcine Gastric Mucin (PGM) Gels. Industrially purified mucin type III (M1778-100G) from porcine stomach was purchased from Sigma-Aldrich (St Louis, MO). Dry mucin powder was dissolved in deionized (Milli-Q) water to a concentration of ~10 mg/mL. The solution was dialyzed using 20 kDa molecular weight cut-off dialysis tubing against four exchanges of distilled water (at 4 °C) to remove salt and low-molecular-weight impurities. Undissolved solids were extracted via centrifugation at 10,000*g* for 10 min at room temperature. The supernatant was frozen in liquid nitrogen and lyophilized. Lyophilized aliquots were stored at −80 °C until use.

CMC sodium salt, average molecular weight = 250 kDa (CAS: 9004-32-4), was purchased from Acros Organics (Thermo Fisher Scientific, Waltham, MA). A solution of CMC in distilled water at 10 mg/mL was dialyzed against distilled water in an Amicon stirred cell (UFSC40001, Amicon) equipped with a 100 kDa molecular weight cut-off membrane. Dialysis was performed with four exchanges of water and the resulting solution was concentrated before lyophilization. Dried CMC was stored at −80 °C until use.

CMC or Sigma PGM was solubilized for up to two nights with gentle shaking at 4 °C in deionized (Milli-Q) water, and gels were prepared the same day as the experiments were performed by combining the solubilized polymers with the appropriate buffers. The pH of the gels was modulated through the addition of a phosphate and sodium citrate buffer to a final concentration of 10 mM both, at an appropriate pH.

Mucin Purification and Reconstitution of Mucin Hydrogels. We considered gels reconstituted to physiological pH levels and mucin concentrations based on literature reports using the three major gel-forming mucins: MUC5B, MUC5AC, and MUC2. We also considered the three native tissues from which mucins are purified: submandibular secretions (MUC5B), gastric mucus (MUC5AC), and intestinal mucus (MUC2). Although our purified MUC5B was not sourced from cervical mucus, we also included cervical mucus as a native mucosal tissue since its primary mucin component is MUC5B.

Porcine-derived mucins were purified from fresh pig stomach scrapings (MUC5AC) or fresh pig intestinal scrapings (MUC2) as previously described.[22] Human-derived MUC5B mucin was purified from submandibular gland secretions following the methods described previously.[23] Briefly, the isolated mucus layer was solubilized in sodium chloride buffer containing protease inhibitors and sodium azide to prevent mucin degradation and bacterial proliferation, respectively,[17] and centrifuged to remove insoluble components. The mucins were isolated using gel filtration chromatography on a Sepharose column (CL2B), and then concentrated, desalted, and lyophilized.[17]

Mucins were solubilized for up to two nights with gentle shaking at 4 °C in deionized (Milli-Q) water, and gels were prepared the same day as the experiments were performed by combining the solubilized mucins with the appropriate reagents. The pH of the gels was modulated through the addition of a phosphate and sodium citrate buffer to a final concentration of 10 mM at the appropriate pH.

In the gastric niche, we compared porcine gastric mucus with MUC5AC gels reconstituted to 5 wt % and at pH 2 to match values reported in the literature for the gastric lumen.[24,25] To assess the importance of the purification method and biochemical structure of the mucins, we also compared these results with Sigma PGM gels reconstituted to the preparation conditions used for the MUC5AC gel. In the intestinal niche, we compared porcine intestinal mucus with MUC2 gels reconstituted to 2.5 wt % (determined as the average of the values cited for porcine small and large intestinal mucus[24]). Although the pH in human intestines has been reported to range from slightly acidic to alkaline (pH 6.4−7.5),[26] we performed our experiments at pH 4 due to the large pH range encountered physiologically during digestion between the stomach and the large intestine.

In the oral niche, we evaluated human saliva versus MUC5B solutions at 0.05 wt % (determined as the approximate average of reported values[27]) and at pH 7 (the published pH range for saliva is 6.2−7.4).[28] Finally, although our purified MUC5B was not sourced from the cervical niche, we compared the response of human cervical mucus with MUC5B gels at 1.5 wt % based on the value reported[29] at both pH 4 and 7. These two pH values were selected due to the variation in the pH of cervical mucus from slightly alkaline[30] (pH 8.6) to acidic (pH 4) in the vagina, after acidification by lactic acid-secreting lactobacilli.[31]

Native Mucus Preparation. Native, whole mucus was collected from four sources: porcine stomach, porcine small intestine, human sublingual gland expressions, and human cervix.

For porcine gastric mucus, previously frozen porcine stomachs were thawed on ice after being delivered frozen from a local slaughterhouse. Stomach contents were emptied and a spatula was used to scrape samples of mucus from the interior epithelium. Stomachs containing blood were discarded and no mucus was collected. After collection, all samples were stored on ice until flash frozen in liquid nitrogen and stored at −80 °C until use. Prior to use, samples were thawed at 4 °C. For porcine intestinal mucus, porcine small intestines were transported on ice from a local slaughterhouse. Intestines were sectioned and loosely adhered mucus was squeezed into a collection vial. Adhered mucus was also collected by cutting each section lengthwise and gently scraping it with a spatula. After collection, all samples were stored on ice until flash frozen in liquid nitrogen and stored at −80 °C until use. Prior to use, samples were thawed at 4 °C.

https://doi.org/10.1021/acs.biomac.2c01016
Biomacromolecules 2023, 24, 628−639

For human sublingual gland expressions, saliva was collected from volunteers after obtaining written informed consent. Salivary secretions were gently suctioned from underneath the tongue into a collection vial on ice. Volunteers had not eaten or consumed fluids for 1 h before saliva collection. Fresh saliva was flash cooled in liquid nitrogen and stored at −80 °C. Saliva samples from 4−6 volunteers were thawed on ice, mixed, and homogenized via shaking at 4 °C for 30 min. Saliva samples were divided into small aliquots to prevent repeated freeze−thaw cycles, flash cooled in liquid nitrogen, and stored at −80 °C until use.

Human cervical mucus was collected from ovulating women at the Women and Infants Hospital of Rhode Island (WHIRI) (WIHRI Approval: WIH 15-0073; MIT Approval: 1501006840R001). Cervical mucus was sampled after obtaining written informed consent and without restrictions on race, ethnicity, or spoken language. Inclusion and exclusion criteria are similar to those used by Smith-Dupont et al.[12] Exclusion criteria were sexually transmitted infection, intercourse within 24 h of collection, abnormal Pap smear within the last 6 months, or cervical surgery within the last 6 months. Patients receiving treatment for infertility and patients with polycystic ovarian syndrome were excluded from the current study.

Samples were collected during a sterile speculum exam, before any other procedure. If present, vaginal fluid or discharge was cleared with a large-tip swab (Scopette). Vaginal fluid clearance does not visually disturb the cervical mucus, which is adherent to the cervical canal.[12] Cervical mucus was collected directly from the external cervical os with a 1 mL insulin syringe. Samples were immediately flash cooled in liquid nitrogen and stored at −80 °C. To minimize freeze−thaw cycles, samples were transported to MIT on ice, divided into smaller volumes, flash cooled in liquid nitrogen, and stored at −80 °C until use. Prior to experiments, samples were thawed at 4 °C.

Macrorheological Experiments. Shear rheology tests were performed using a strain-controlled ARES-G2 rheometer (TA Instruments, New Castle, DE) with an 8 mm parallel plate fixture with a truncation gap of 200 μm. Approximately 15 μL of solution was used for each experiment. All experiments were performed on a Peltier plate at 25 °C. SAOS measurements were performed at a strain amplitude within the linear viscoelastic regime of each sample, as determined from separate strain sweep experiments (data not shown).

For all experiments, a thin coating of mineral oil was placed around the edge of the sample to prevent evaporation. Data points for the mucin, Sigma PGM, and CMC gels denote the average of "up" and "down" frequency sweeps for a single sample, with the standard deviation between these measurements shown. For the native mucus, data points denote the average and standard deviation of 1−2 tissue samples, including averaging over up and down frequency ramps. For clarity, only the positive error bars are shown due to the logarithmic nature of the plots.

SPT Experiments. *Experimental Protocol.* SPT samples were prepared by combining the mucin gels or native mucus with a microsphere solution at a volume ratio of 60:1 (mucin gel/mucus: microsphere solution). The microsphere solution was composed of fluorescent, negatively charged (carboxylated) microspheres 1 μm in diameter (Magsphere, Inc., Cat No. CAF-001UM, Pasadena, CA) diluted in Milli-Q water at a volume ratio of 1:200. This strategy resulted in an overall dilution ratio of 1:12,000 for the microspheres. Negatively charged particles were used based on previous findings of increased charge-mediated diffusion impairment for positively charged (amine functionalized) particles in comparison to negatively charged (carboxylated or sulfated) ones in mucus and mucin gels.[32,33] All samples were subsequently vortexed for ∼10 s to ensure adequate mixing, and then ∼25 μL of the sample was pipetted into borosilicate square capillaries 0.9 mm × 0.9 mm in cross section (#8290; Vitrocom, Mountain Lakes, NJ) to fill the tube completely. Capillaries were sealed on both ends using a 1:1:1 mixture of petroleum jelly, lanolin, and paraffin and then mounted onto microscope slides for imaging. For the mucin, Sigma PGM, and CMC gels, three experimental replicates were performed for each condition. Sufficient sample was prepared to perform SPT in three separate particle-laden capillaries. For native mucus, the number of specimens measured varied between 1 and 3 depending on sample availability, and the number of experiments performed varied between 3 and 6.

Imaging was performed at 30.3 frames per second for 10 s and at room temperature with a Zeiss Axio Observer D.l. inverted microscope using a Zeiss LD Plan-Neofluar 20×/0.4 Corr Ph2 objective lens (Carl Zeiss Microscopy GmbH, Jena, Germany) and a Hamamatsu Flash 4.0 Cl 1440- 22CU camera (Hamamatsu Photonics, Hamamatsu City, Japan). An average of 186 particles were imaged for each specimen from an average of seven movies recorded at distinct locations within the glass capillaries. For each image frame, particles were identified using publicly available MATLAB (Natick, MA) code that identifies candidate features using high-intensity matches and filtering them using criteria such as maximum feature eccentricity and radius of gyration.[34,35]

Analysis. The x and y positions of every validated particle in each frame were recorded using the same publicly available MATLAB code by the center of mass of the localized image intensity. A drift correction code from the same publicly available source[34] was subsequently applied to all SPT data. This correction subtracts the center-of-mass motion of all of the particles in a given frame from each individual trajectory. Using these drift-corrected data, the time-averaged mean squared displacement (MSD; in one dimension) of the kth particle for a movie N images in length is given by[22,36]

$$\overline{\Delta x_k^2\,(\Delta\tau)} = \frac{1}{N - \frac{\Delta\tau}{\Delta t}} \sum_{i=1}^{N-\Delta\tau/\Delta t} [(x_k(i\Delta t + \Delta\tau) - x_k(i\Delta t))^2] \tag{1}$$

where Δt is the time between successive frames and $\Delta\tau$ is the lag time. The ensemble-average MSD over all K particles is then

$$\langle \Delta x^2(\Delta\tau)\rangle = \frac{1}{K}\sum_{k=1}^{K} \overline{\Delta x_k^2\,(\Delta\tau)} \tag{2}$$

For normal diffusive motion such as that occurring in a homogeneous Newtonian medium with no fluid memory and with which the microspheres do not interact, the MSD is expected to scale linearly with lag time, and in one dimension the explicit form of this scaling[36] is

$$\langle \Delta x^2(\Delta\tau)\rangle = 2D\Delta\tau \tag{3}$$

where D is the translational diffusion coefficient of the microsphere in the medium. This normal diffusion is known as Brownian motion, and when this scaling does not hold, the diffusion is termed *anomalous* or *non-Brownian*,[36] and the MSD is generally expressed as an arbitrary, monotonically increasing function of the lag time, often assigned a power-law form as

$$\langle \Delta x^2(\Delta\tau)\rangle = 2D_\alpha \Delta\tau^\alpha \tag{4}$$

where D_α is a generalized diffusion coefficient.[37] When $\alpha < 1$, the motion of the particle is subdiffusive, and when $\alpha > 1$, the motion is superdiffusive.[36] The one-dimensional step size distribution for a random walk at a given lag time $\Delta\tau$ is a Gaussian distribution[37] about a displacement $\Delta x = 0$

$$P(\Delta x, \Delta\tau) = \frac{1}{\sqrt{4\pi D\Delta\tau}} e^{-\Delta x^2/4D\Delta\tau} \tag{5}$$

where, as before, D is the diffusion coefficient of the walker in the medium. For a Gaussian distribution, the kurtosis (or ratio of the 4th moment to the 2nd moment of the distribution) is calculated to be

$$\beta = \frac{\langle \Delta x^4\rangle}{\langle \Delta x^2\rangle^2} = 3 \tag{6}$$

and hence following Evers et al.,[38] we define a suitable non-Gaussian parameter κ as

$$\kappa = \frac{\langle \Delta x^4\rangle}{3\langle \Delta x^2\rangle^2} - 1 \tag{7}$$

https://doi.org/10.1021/acs.biomac.2c01016
Biomacromolecules 2023, 24, 628−639

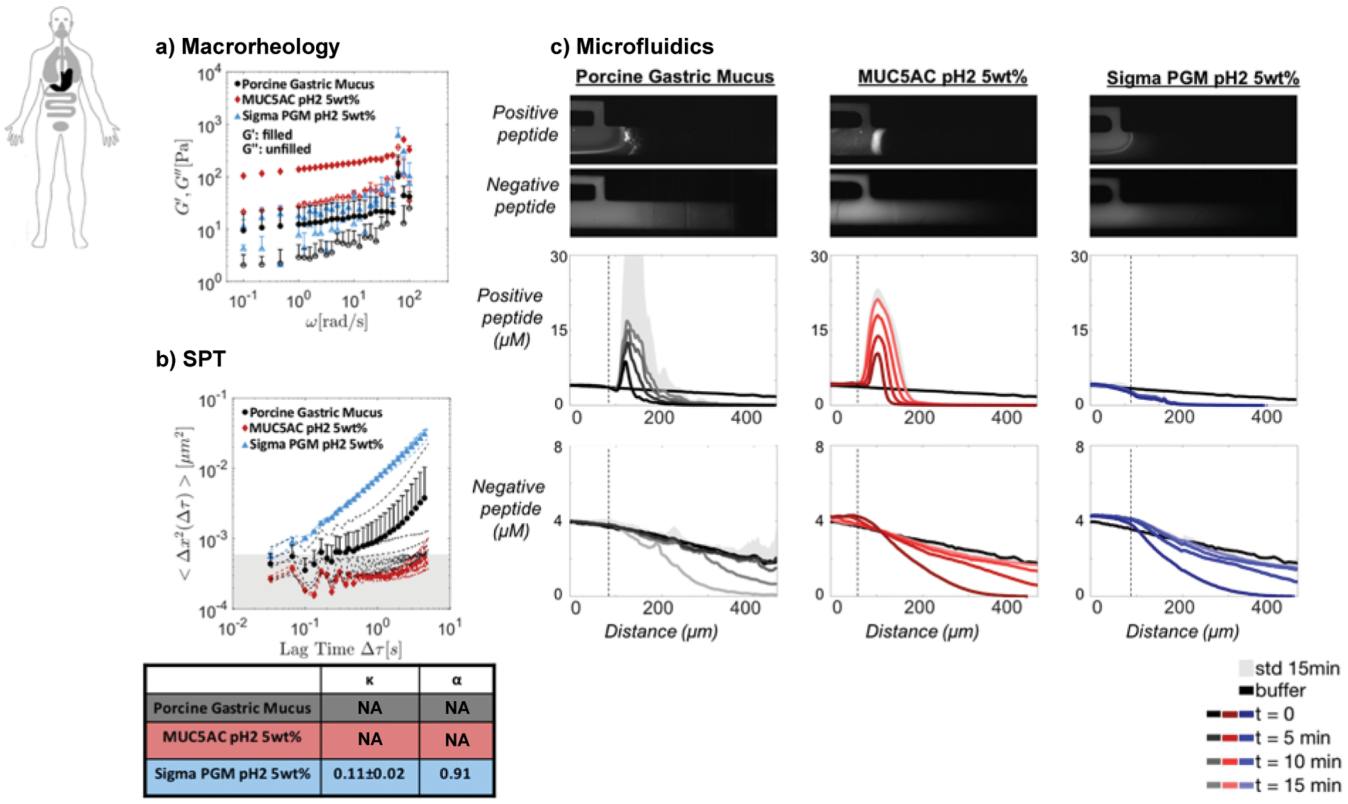

	κ	α
Porcine Gastric Mucus	NA	NA
MUC5AC pH2 5wt%	NA	NA
Sigma PGM pH2 5wt%	0.11±0.02	0.91

Figure 3. Comparison between gastric mucus, 5 wt % MUC5AC at pH 2, and 5 wt % Sigma PGM at pH 2. (a) Macrorheological SAOS data. Filled symbols denote the storage modulus G' and unfilled symbols denote the loss modulus G''. (b) SPT data. Dashed lines denote the ensemble-average MSD of an individual experiment, filled symbols denote the average over all experiments, and the gray area denotes the estimated static error of the experimental setup. Values of the non-Gaussian parameter κ measured at a delay time of $\Delta\tau$ = 0.1 s are provided, along with the anomalous diffusion exponent α, for data lying above the noise floor. (c) Microfluidic peptide diffusion assay. Microscope images of representative diffusion channels at t = 15 min after positive or negative peptide introduction (top). Averaged concentration profiles calculated for the diffusion channels at t = 1, 5, 10, and 15 min (bottom). Diffusion of the probe into the buffer is presented in black.

For normal Brownian motion, we expect $\kappa \ll 1$. Deviations from this expression are frequently attributed to heterogeneity of the surrounding medium.[38]

Analysis of Matrix Interactions. *Experimental Protocol.* To serve as probes in a procedure conceptually analogous to affinity chromatography, two peptides, AK_{10} ($Y(AK)_{10}$-NH_2) and AE_{10} ($Y(AE)_{10}$-NH_2), were synthesized using the solid phase synthesis method and labeled post-synthesis with a (5-)6-tetramethylrhodamine (TAMRA) fluorophore at the N-terminus. Peptides were purified using reverse-phase high-performance liquid chromatography. Peptide identity and extent of labeling were confirmed using matrix-assisted laser desorption ionization mass spectrometry. Synthesis, purification, and identification for both peptides were performed by the Swanson Biotechnology Center at the Koch Institute at MIT (Cambridge, MA). Peptides were dissolved to a final concentration of 4 μM in a buffer containing 20 mM 4-(2-hydroxyethyl)-1-piperazineethanesulfonic acid (HEPES) at pH 7 and 20 mM NaCl (buffer H7). For native mucus samples, mucin, Sigma PGM, and CMC gels, two experimental replicates were performed for each condition. Sufficient sample was prepared to measure transport in at least two separate microfluidic devices, and data was collected from 4−8 channels for each peptide.

Microfluidic devices were designed and fabricated from polydimethylsiloxane as previously described.[39,40] Devices were cured at 9 °C for 48−72 h after fabrication. For the microfluidic diffusion assay, as previously described,[12] devices were bonded to microscope slides and imaged with a Zeiss Observer Zl inverted epifluorescence microscope equipped with a 5× objective and mercury lamp source. The incident light source was filtered to 568 nm to selectively excite the (5-)6-tetramethylrhodamine fluorophore. Mucus or mucin gels were injected into the main channel. The bottom valve was closed to prevent flow out of the main channel. Buffer H7 was used to wash the inlet and outlet channels. Twenty-five microliters of 4 μM peptide solution was added to the inlet reservoir and allowed to flow via gravitational flow. An image was acquired every 10 s for 120 frames (20 min). Experiments were performed at least in duplicate.

Analysis. Images were analyzed and quantified using previously described methods[12] with ImageJ (vl.47; Wayne Rasband, National Institutes of Health, Bethesda, MD; http://imagej.nih.gov/ij and v8.2.0.701; Natick, MA) software. Concentration profiles from separate runs were manually aligned as previously reported.[12] Average profiles were calculated after alignment, for t = l, 5, 10, and 15 min, for each preparation or specimen. For clarity, only the positive standard deviations of t = 15 min are shown in Figures 3−6.

RESULTS AND DISCUSSION

We determined the macrorheological (SAOS) and SPT responses of the mucus and mucin gels for each physiological niche considered, along with the corresponding value of the non-Gaussian parameter κ at a lag time of $\Delta\tau$ = 0.1 s and the slope of the MSD fit between lag times of 0.03 s $\leq \Delta\tau \leq$ 5 s (Figures 3−6). We also employed a microfluidic device to evaluate the diffusion of positively and negatively charged peptide probes into the mucus and mucin gels for each physiological niche.

Gastric Niche. Reconstituted MUC5AC gels were stiffer macroscopically than gastric mucus (Figure 3a), yet the response of both materials was predominantly solid-like ($G' > G''$), with both moduli exhibiting weak power-law dependencies on the oscillation frequency (ω), a characteristic of

https://doi.org/10.1021/acs.biomac.2c01016
Biomacromolecules 2023, 24, 628−639

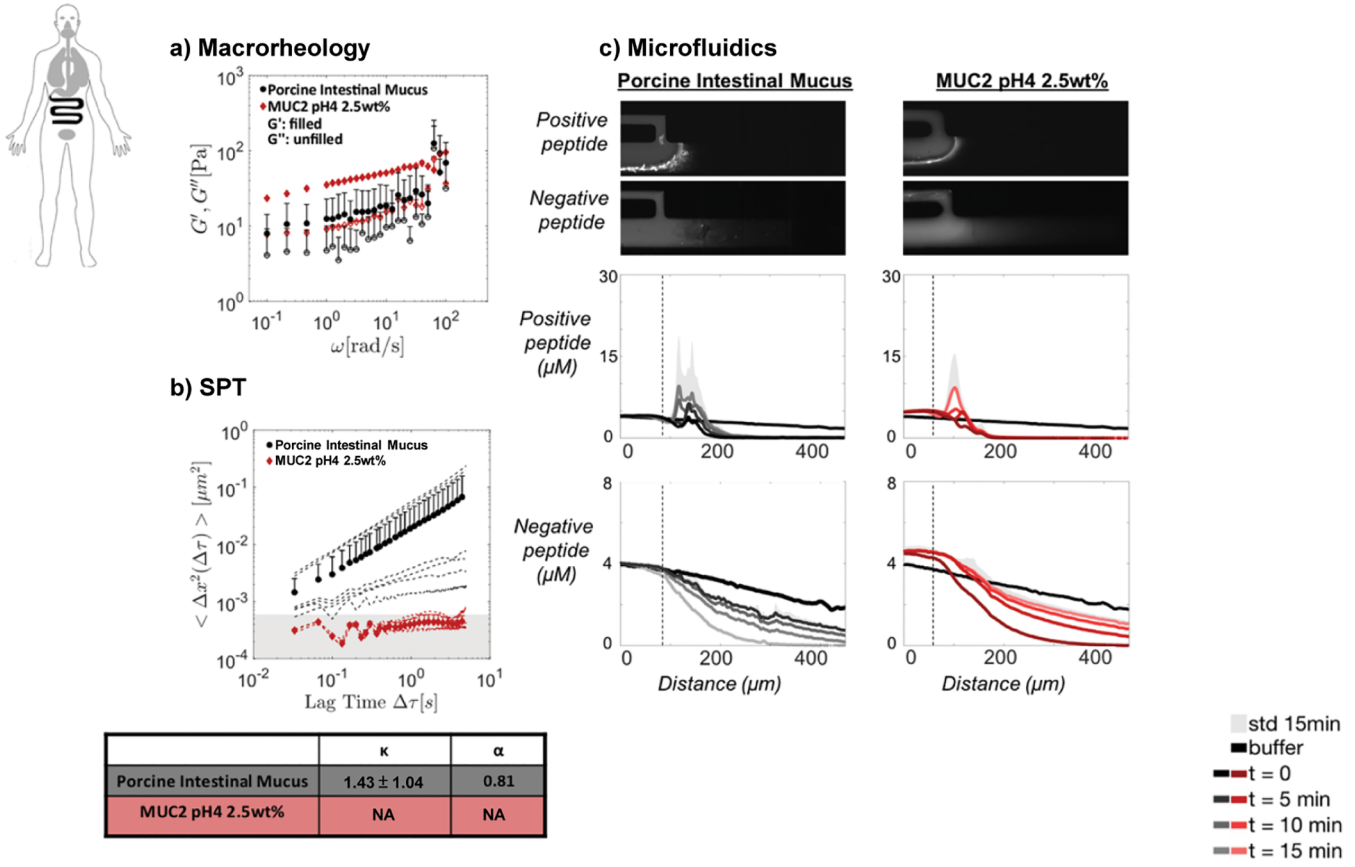

	κ	α
Porcine Intestinal Mucus	1.43 ± 1.04	0.81
MUC2 pH4 2.5wt%	NA	NA

Figure 4. Mucin purified from the intestinal niche displays characteristics similar to those of intestinal mucus. Comparison between intestinal mucus and 2.5 wt % MUC2 at pH 4. (a) Macrorheological SAOS data. Filled symbols denote the storage modulus G' and unfilled symbols denote the loss modulus G''. (b) SPT data. Dashed lines denote the ensemble-average MSD of an individual experiment, filled symbols denote the average over all experiments, and the gray area denotes the static error of the experimental setup. Values of the non-Gaussian parameter κ measured at a delay time of $\Delta\tau = 0.1$ s are provided, along with the anomalous diffusion exponent α, for data lying above the noise floor. (c) Microfluidic peptide diffusion assay. Microscope images of representative diffusion channels at $t = 15$ min after positive and negative peptide introduction (top). Averaged concentration profiles calculated for the diffusion channels at $t = 1$, 5, 10, and 15 min (bottom). Diffusion of the probe into the buffer is presented in black.

cross-linked gels with multiple length and time scales.[41] As evident from the ensemble-average MSD of the individual experiments (dashed lines in Figure 3b), the SPT results for these two samples were similar to each other, with the exception of one experimental replicate in gastric mucus for which unusually large particle displacement was observed. This large variation between native mucus samples was reflected in the substantially higher value of κ (and its standard deviation) for gastric mucus ($\kappa = 0.86 \pm 1.18$—reported as NA in Figure 3b, data below experimental static error limit) compared to the MUC5AC gel ($\kappa = 0.04 \pm 0.04$—reported as NA in Figure 3b, data below experimental static error limit). It is important to note that SPT measurements for both samples lay within the limit of the measured static error of the experimental setup, as previously quantified by measuring the MSD of sample particles "immobilized" in a 3 wt % agarose gel.[42] Hence, the MSD measurements for both of these experiments should not be interpreted quantitatively. Macroscopically, the stiffness of the Sigma PGM gel was nearly an order of magnitude lower than that of the MUC5AC gel, and the Sigma PGM also exhibited power-law dependencies of its moduli on ω (Figure 3a). Microscopically, as with the MUC5AC gel, the particle trajectories in the Sigma PGM gel were also quite homogeneous ($\kappa = 0.11 \pm 0.02$; Figure 3b). However, unlike in the MUC5AC gel and in gastric mucus, the particle motion in the Sigma PGM gel was weakly subdiffusive ($\alpha = 0.91$). This difference in transport is in accordance with differences in the microstructure,[43] which may further explain why distinct microbial behaviors in native mucin are not recapitulated by commercially available mucin.[17,44]

In both gastric mucus and the reconstituted MUC5AC gels, the concentration profile of the positively charged peptide exhibited a peak at the mucus−buffer interface (Figure 3c). This enrichment reflects an accumulation of the peptide in the mucus matrix, likely arising from electrostatic interactions between the positive peptide and the negatively charged mucin molecules, as previously observed in mucin gels.[40] In contrast, the concentration of the negative peptide decreased along both the reconstituted MUC5AC gel (Figure 3c) and along gastric mucus channels in the microfluidic device in a way similar to the free diffusion of this particle in buffer (Figure 3c), demonstrating that interactions between the negative peptides and mucus (with mucins in particular) were rather weak. Similar transport profiles of both peptide probes in gastric mucus and the MUC5AC gel (Figure 3c) suggest that the biochemical properties relevant to the transport of charged nanoscale molecules are similar in these two materials. However, the transport profiles of both peptides were notably

https://doi.org/10.1021/acs.biomac.2c01016
Biomacromolecules 2023, 24, 628−639

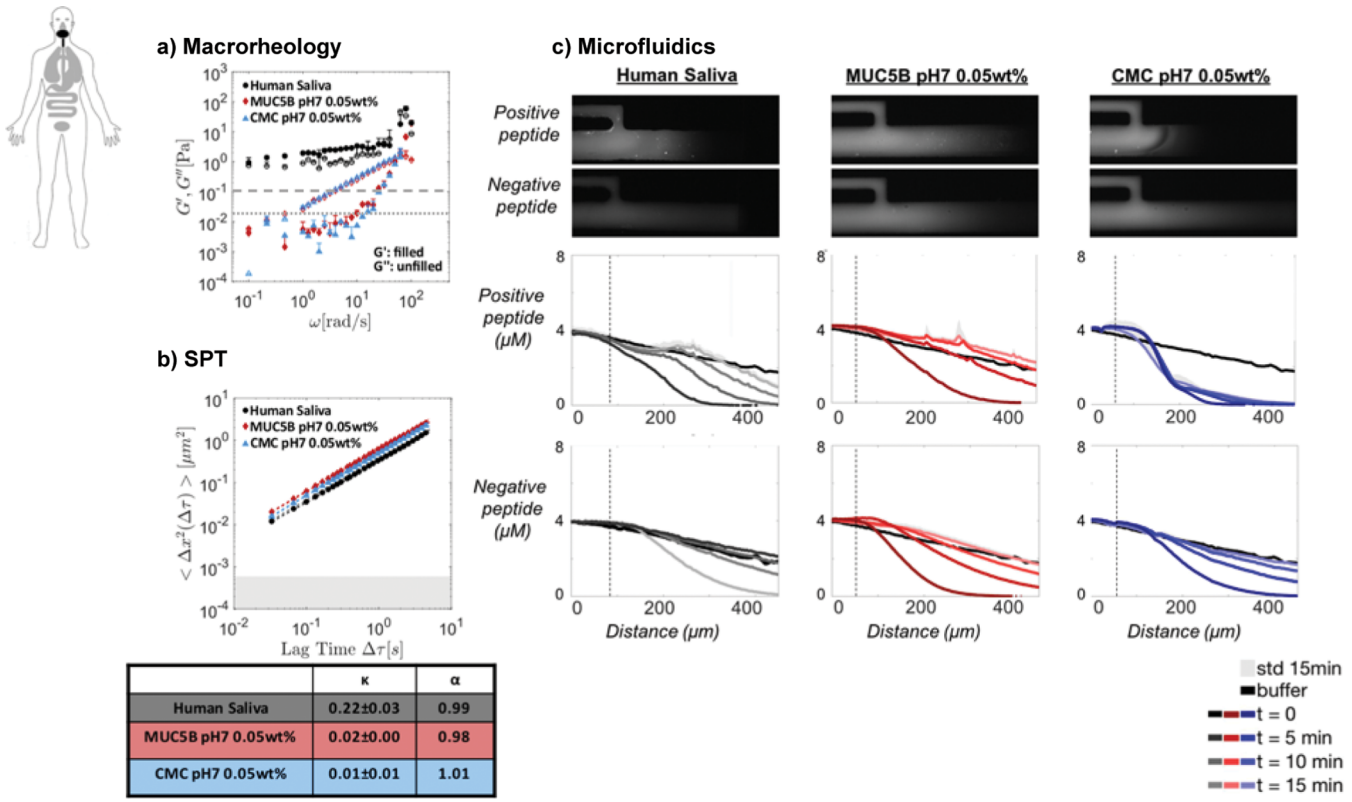

	κ	α
Human Saliva	0.22±0.03	0.99
MUC5B pH7 0.05wt%	0.02±0.00	0.98
CMC pH7 0.05wt%	0.01±0.01	1.01

Figure 5. Mucin purified from the oral niche does not exhibit characteristics identical to those of saliva. Comparison between human saliva, 0.05 wt % MUC5B at pH 7, and 0.05 wt % CMC at pH 7. (a) Macrorheological SAOS data. Filled symbols denote the storage modulus G' and unfilled symbols denote the loss modulus G″. The gray long dashed lines denote the instrument torque limit based on the manufacturer's specifications, and the short dashed lines the minimum torque limit obtained from previous experiments performed in our group. (b) SPT data. Dashed lines denote the ensemble-average MSD of an individual experiment, filled symbols denote the average over all experiments, and the gray area denotes the static error of the experimental setup. Values of the non-Gaussian parameter κ measured at a delay time of $\Delta\tau$ = 0.1 s are provided, along with the anomalous diffusion exponent α. (c) Microfluidic peptide diffusion assay. Microscope images of representative diffusion channels at t = 15 min after positive and negative peptide introduction (top). Averaged concentration profiles calculated for the diffusion channels at t = 1, 5, 10, and 15 min (bottom). Diffusion of the probe into the buffer is presented in black.

less smooth in gastric mucus than in the MUC5AC gel (Figure 3c), which is consistent with the presence of additional non-mucin components and a more heterogeneous microstructure in gastric mucus. In the reconstituted Sigma PGM gel, the positive peptide yielded a smaller enrichment peak at the interface than gastric mucus and the reconstituted MUC5AC gel, while the negative peptide was transported in a manner similar to that observed in gastric mucus (Figure 3c). This difference in the concentration profiles (particularly of the positive peptide) between the Sigma PGM and MUC5AC gels (Figure 3c) likely reflects structural and biochemical changes to the mucin molecules arising from variations in the purification protocols of the polymers.

In short, the reconstituted MUC5AC gels exhibit similar rheological and biochemical properties to gastric mucus samples unlike the properties measured in Sigma PGM. The purification processes of mucins should be carefully considered as they may substantially alter the final mucin product and care should be taken in interpreting experimental findings depending on the type of mucin used. Indeed, studies have reported varying similarity between native mucus and reconstituted mucin gels when using different measurement techniques, environmental conditions,[45] purification methods,[27,45,46] and mucosal niches. Gels reconstituted from Sigma PGM undergo a certain degree of proteolytic digestion during their harsh commercial purification process and consequently do not exhibit pH responsiveness.[4,47] As a consequence, Sigma PGM gels have been shown to not be accurate models for porcine intestinal mucus based on the diffusion of drug molecules[48] and 200 nm polystyrene particles with a variety of surface chemistries.[31] MUC5AC hydrogel response was predominantly solid-like ($G' > G''$) and showed subdiffusive particle motion, similar to gastric mucus (Figure 3a,b), although substantial variation between samples was observed in the native mucus. The MUC5AC mucin forms a selective hydrogel, with two distinct transport behaviors of permeability or retention, exhibited also by gastric mucus. The negative analyte is transported into the gel, while the positive analyte is retained at the gel interface (Figure 3c). On the other hand, Sigma mucin was an order of magnitude less stiff (Figure 3a), had weaker subdiffusive motion (i.e., MSD slopes were closer to the normal diffusion limit of α = 1) (Figure 3b), and retained less positive peptide (Figure 3c).

Intestinal Niche. Similar to gastric mucus, substantial variations in the micro- and macrorheology of native intestinal mucus were observed between samples (Figure 4). However, macroscopically, both the MUC2 gel and the native mucus sample showed similar weak power-law dependencies of G' and G'' on ω and both were predominantly solid-like ($G' > G''$; Figure 4a). Microscopically, the MUC2 gel again exhibited fairly homogeneous particle trajectories (κ = 0.14 ± 0.18—reported as NA in Figure 4b, data below experimental static

https://doi.org/10.1021/acs.biomac.2c01016
Biomacromolecules 2023, 24, 628−639

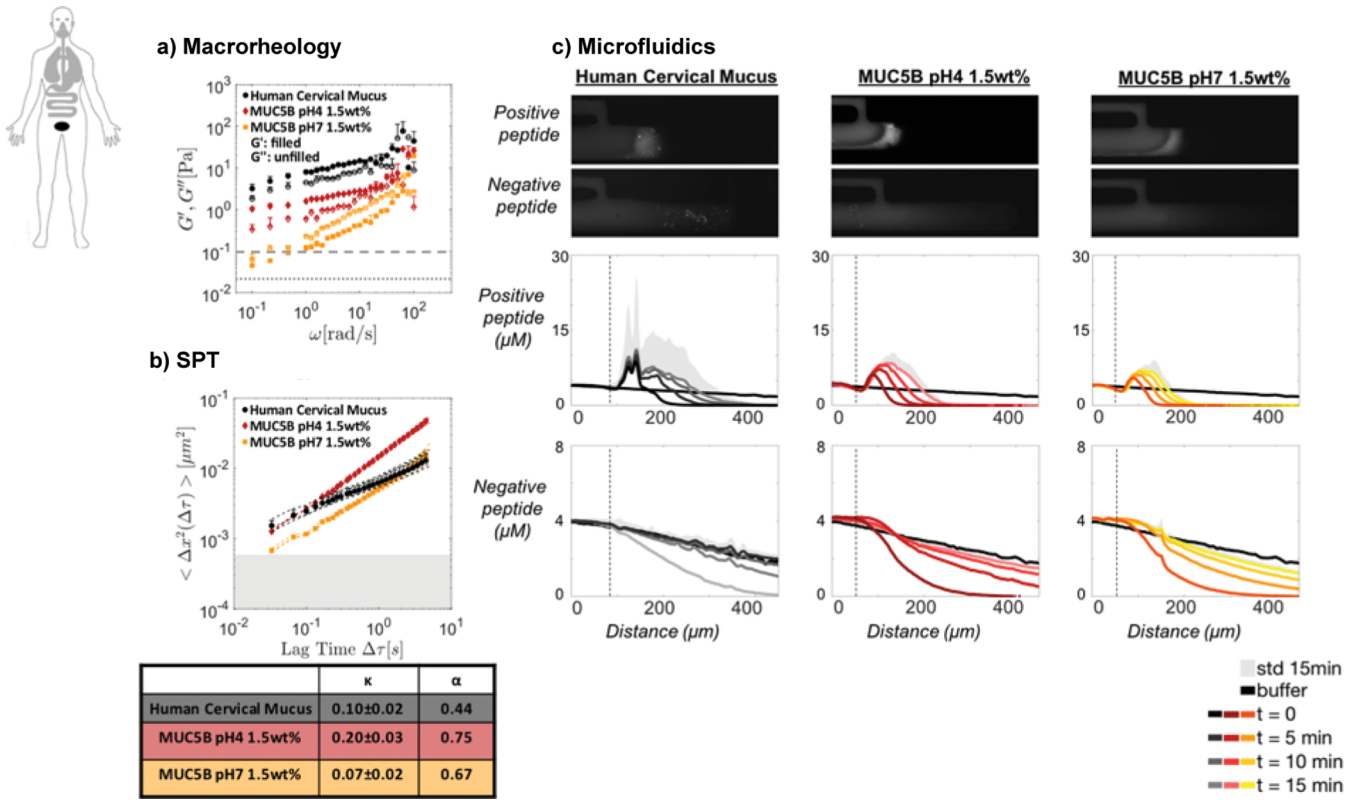

	κ	α
Human Cervical Mucus	0.10±0.02	0.44
MUC5B pH4 1.5wt%	0.20±0.03	0.75
MUC5B pH7 1.5wt%	0.07±0.02	0.67

Figure 6. Mucin purified from the oral niche can display characteristics similar to those of cervical mucus. Comparison between human cervical mucus, 1.5 wt % MUC5B at pH 4, and 1.5 wt % MUC5B at pH 7. (a) Macrorheological SAOS data. Filled symbols denote the storage modulus G' and unfilled symbols denote the loss modulus G''. The gray long dashed lines denote the instrument limit based on the manufacturer's minimum torque limit and the short dashed lines denote the experimental limit. (b) SPT data. Dashed lines denote the ensemble-average MSD of an individual experiment, filled symbols denote the average over all experiments, and the gray area denotes the static error of the experimental setup. Values of the non-Gaussian parameter κ measured at a delay time of $\Delta\tau = 0.1$ s are provided, along with the anomalous diffusion exponent α. (c) Microfluidic peptide diffusion assay. Microscope images of representative diffusion channels at $t = 15$ min after positive and negative peptide introduction (top). Averaged concentration profiles calculated for the diffusion channels at $t = 1$, 5, 10, and 15 min (bottom). Diffusion of the probe into the buffer is presented in black.

error limit) and strongly subdiffusive motion ($\alpha = 0.14$—reported as NA in Figure 4b, data below experimental static error limit) (Figure 4b). As with the MUC5AC gel, care should be taken in interpreting these results quantitatively because the data lay below the estimated static error of the experimental setup. The SPT of the native specimens varied substantially between samples ($\kappa = 1.43 \pm 1.04$), although several specimens also harbored strongly subdiffusive particle motion (Figure 4b).

Both intestinal mucus and reconstituted MUC2 gels were enriched for the positive peptide at the mucus−buffer interface (Figure 4c), similar to gastric mucus and MUC5AC gels (Figure 3c). The presence of numerous peaks in the transport profile of the positive peptide in intestinal mucus reflects the higher degree of structural complexity in this material compared to the purified MUC2 gel and may arise from interactions between the positive peptide and additional nonmucin components. The positive peptide concentration profile in MUC2 had a smoother, singular enrichment peak due to the more homogeneous content and structure of this sample (Figure 4c). The negative peptide established a decreasing concentration gradient in both materials reminiscent of the free diffusion observed in the buffer (Figure 4c). However, unlike in MUC2 gels, we detected small fluctuations in the transport profile of the negative probes in intestinal mucus, as well as brighter patches in the images of the channels (Figure 4c). These observations highlight weak interactions between the negative peptides and the structurally heterogeneous intestinal mucus samples, which were absent from MUC2 gels (Figure 4c), that feature a more homogeneous polymer makeup and a simpler hydrogel structure. However, we observed mild enrichment of the negative peptide at the MUC2 gel interface, which may result from partitioning of the probe due to the positive charges on mucin molecules.

Taken together, the experimental evidence shows that gels reconstituted from MUC2 had similar rheological and biochemical properties to the intestinal mucus samples, although substantial heterogeneity in native intestinal mucus samples resulted in both qualitative and quantitative differences, particularly in the observed rheology. The MUC2 mucin hydrogel was predominantly solid-like and exhibited subdiffusive motion of microspheres, largely similar to intestinal mucus (Figure 4a,b). The MUC2 hydrogel accumulates positive peptide at the interface, and is permeable to the negative peptide, exhibiting a similar transport pattern to the intestinal mucus (Figure 4c).

Oral Niche. The macroscopic rheological responses of MUC5B and CMC solutions were both qualitatively and quantitatively different from those of human whole saliva. In particular, saliva displayed the characteristic trends observed in other native mucus samples of weak power-law dependencies of the moduli on ω ($G' > G''$) (Figure 5a). In response to

https://doi.org/10.1021/acs.biomac.2c01016
Biomacromolecules 2023, 24, 628−639

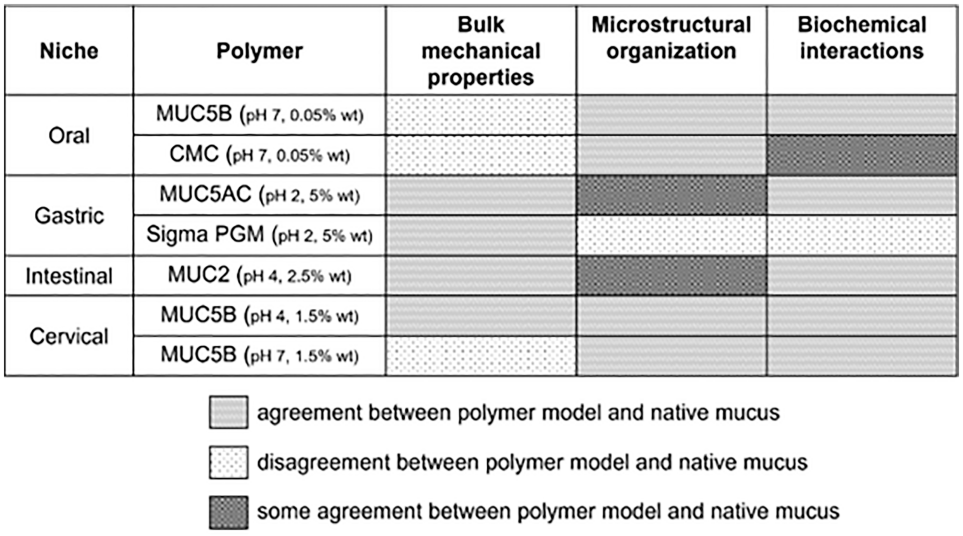

Figure 7. Summary of the qualitative and semiquantitative agreement in bulk mechanical properties agreement in microstructural organization and biochemical interactions between various polymer models and native mucus for the studied niches.

small-amplitude oscillatory shear deformations, both the MUC5B and CMC solutions responded essentially as liquids, with a linear dependence of the loss modulus on frequency and an elastic modulus lying within the low-torque limit of the instrument at low frequencies (Figure 5a); this modulus had a quadratic dependency on ω at high frequencies (Figure 5a), a signature of fluid inertial effects.[49] This observation suggests that unlike in other native mucus samples, the very low salivary MUC5B concentrations of ~0.05 wt % cannot fully account for the weak-gel rheological response of saliva, and that other components such as non-mucin proteins and salivary micelles may play an important role.[28] Microscopically, diffusive particle motion ($\alpha \approx 1$) occurred in all three materials along with homogeneous particle motion, with the human whole saliva sample exhibiting the largest degree of heterogeneity ($\kappa = 0.22 \pm 0.03$) (Figure 5b). In human saliva, the concentration profile of the positive peptide featured a small initial decrease followed by a mild enrichment at the mucus−buffer interface (Figure 5c). A similar profile was observed in the 0.05 wt % MUC5B gel (Figure 5c), although we noted that working with such low polymer concentrations presented difficulties at the washing and loading stages of the microfluidic experiments. Nearly free diffusion of the positively charged peptide occurred in the remainder of the microfluidic channel for both saliva and the MUC5B gels (Figure 5c). In contrast, the 0.05 wt % CMC gel formed a stronger biochemical barrier at the gel−buffer interface, which resulted in a steeper drop in the concentration of the positive peptide away from the interface and strongly inhibited diffusion of this probe into the remainder of the channel (Figure 5c). This difference is likely due to the stronger anionic character of CMC compared to MUC5B. For the negatively charged peptide, a transport profile indicative of nearly free diffusion was detected in all three samples (Figure 5c).

In brief, the reconstituted MUC5B gels did not have similar macrorheological properties to human whole saliva, although they had similar microrheological and biochemical characteristics. The MUC5B hydrogel responded as a liquid unlike the weak-gel response of the saliva samples (Figure 5a). Both the MUC5B gel and saliva had diffusive motion of microspheres (Figure 5b) and a weak enrichment of the positive peptide at the gel interface (Figure 5c). The CMC gel responded as a liquid rheologically (Figure 5a), had diffusive motion of particles (Figure 5b) and was less permeable to the positive analyte (Figure 5c). All considered, MUC5B hydrogels can simulate transport in saliva. However, both MUC5B and CMC could not reconstitute the saliva gel-like response at the low polymer concentration of 0.05 wt %.

Cervical Niche. In the cervical niche, similar weak power-law responses were observed in the moduli of cervical mucus as well as the MUC5B gels, although the reconstituted gels were softer than the native sample at both pH levels (Figure 6a). The pH sensitivity of the purified mucin gels was keenly demonstrated in this niche by the predominantly liquid-like response of the gel at pH 7 ($G' < G''$) and solid-like response at pH 4 ($G' > G''$, Figure 6a). The biochemical mechanism underlying this pH dependence has been studied in detail for MUC5AC;[20,47] this dependence is believed to be due to the unfolding of nonglycosylated domains on mucin molecules under acidic conditions, which exposes previously hidden hydrophobic moieties that facilitate the formation of additional cross-links between the hydrophobic domains at lower pH.[4,20] Microscopically, all three samples led to fairly homogeneous particle trajectories (with $\kappa = 0.10 \pm 0.02$ for the native mucus sample, Figure 6b), as well as subdiffusive MSD scalings to various degrees ($\alpha = 0.44$ for cervical mucus, $\alpha = 0.75$ for MUC5B at pH 4, and $\alpha = 0.67$ for MUC5B at pH 7) (Figure 6b). Interestingly, the particles were less mobile in the MUC5B gels at pH 7 than at pH 4, although these neutral samples appeared to be softer macrorheologically.

In cervical mucus, a wide peak in the concentration of the positively charged peptide occurred at the mucus−buffer interface (Figure 6c). This broad peak was also evident in the MUC5B gels at both pH 4 and 7 (Figure 6c), which is suggestive of similar biochemical and structural environments between the native and reconstituted samples. Note, however, that the concentration of the positive peptide at the gel−buffer interface was higher in the MUC5B gel at pH 4 than at pH 7 (Figure 6c). Similar to the other physiological niches, nearly free diffusion of the negatively charged peptides was observed in all three gels from the cervical niche.

https://doi.org/10.1021/acs.biomac.2c01016
Biomacromolecules 2023, 24, 628−639

In short, the reconstituted MUC5B gels possess similar rheological and biochemical properties to the cervical mucus samples, particularly under acidic conditions (pH = 4). At pH 4, similar to the cervical mucus samples, MUC5B mucin gels had a predominantly solid-like macrorheological response, and subdiffusive particle motion (Figure 6a,b). MUC5B gels had similar permeability properties to cervical mucus, particularly under more acidic conditions (Figure 6c).

CONCLUSIONS

Here, we employed a variety of biophysical measurements to assess and compare the physicochemical properties of native mucus with gels reconstituted from natively purified mucins, commercial mucins, and synthetic polymers. We found that across niches under certain conditions, reconstituted mucin gels and, less frequently, commercial mucins such as Sigma PGM or mucin substitutes such as CMC could qualitatively and semiquantitatively reproduce properties of native mucus. Our findings are summarized in Figure 7. We note that other physiologically relevant parameters such as lubricity,[50] which we did not measure, can also be important to consider when considering *in vitro* mucus models. The nonnegligible variations between native mucus samples, particularly seen in the intestinal and gastric niches, complicate the drawing of quantitative conclusions about the rheological responses of mucus and mucin gels. Further, our use of literature values for the pH levels and mucin concentrations of the reconstituted mucin gels also excludes the possibility of quantitatively comparing the responses of these materials with those of native mucus, which could be of interest in a broader study regarding the cause of variation between mucus samples. In addition to pH and concentration of mucin hydrogels assayed here, mucus properties are further modulated by the presence of lipids and proteins found in mucus,[51,52] which could explain a higher variability in mucus samples, compared to mucin gels.

The ability to represent all aspects of mucus in one experimental model, including its mechanical, biological, and chemical properties, is experimentally challenging because it requires the model to be representative across multiple length scales. However, modeling a specific application or physiological feature of mucus may not require accuracy at all length scales. For example, in the context of large-scale phenomena such as mucus clearance, the macrorheological properties of native mucus may be the most crucial to model to study physical processes like fragmentation and dispersion. On the other hand, a mucus model system that exhibits native mucus' "stickiness", permeability, and related biochemical properties may be appropriate for the systematic study of comparatively small-scale processes such as the transport of biological substances (e.g., bacteria, viruses, drug-delivery vehicles) through the mucus barrier.

To conclude, model mucus systems may allow us to better understand the role of mucus permeability and barrier function in health and disease. Even lab-purified mucins that successfully retain specific physiological features may not represent native mucus well in all applications. With this in mind, establishing the characteristic length scale of the system or of the process being studied can guide the selection of the appropriate mucin polymer model system (lab-purified mucin, commercial mucin, or synthetic mucin) that should be used to best capture the critical features of native mucus that are being investigated.

AUTHOR INFORMATION

Corresponding Authors

Caroline E. Wagner − *Department of Mechanical Engineering, Massachusetts Institute of Technology, Cambridge, Massachusetts 02139, United States;* Present Address: Department of Bioengineering, McGill University, Montreal, Canada H3A 0E9; orcid.org/0000-0001-5193-2797; Email: caroline.wagner@mcgill.ca

Katharina Ribbeck − *Department of Biological Engineering, Massachusetts Institute of Technology, Cambridge, Massachusetts 02139, United States;* orcid.org/0000-0001-8260-338X; Phone: +1 (617) 715-4575; Email: ribbeck@mit.edu

Authors

Miri Krupkin − *Department of Biological Engineering, Massachusetts Institute of Technology, Cambridge, Massachusetts 02139, United States;* Present Address: Department of Structural Biology, Stanford University, Stanford, California 94305, United States.; orcid.org/0000-0002-5917-0894

Kathryn B. Smith-Dupont − *Department of Biological Engineering, Massachusetts Institute of Technology, Cambridge, Massachusetts 02139, United States;* Present Address: Vertex Pharmaceuticals, Incorporated, Boston, Massachusetts 02210, United States.

Chloe M. Wu − *Department of Biological Engineering, Massachusetts Institute of Technology, Cambridge, Massachusetts 02139, United States;* orcid.org/0000-0002-8451-1718

Nicole A. Bustos − *Department of Mechanical Engineering, Massachusetts Institute of Technology, Cambridge, Massachusetts 02139, United States;* orcid.org/0000-0002-3074-5957

Jacob Witten − *Department of Biological Engineering and Computational and Systems Biology Initiative, Massachusetts Institute of Technology, Cambridge, Massachusetts 02139, United States;* Present Address: Department of Chemical Engineering, Massachusetts Institute of Technology, Cambridge, Massachusetts 02139, United States; David H Koch Institute for Integrative Cancer Research, Massachusetts Institute of Technology, Cambridge, Massachusetts 02139, United States.

Complete contact information is available at: https://pubs.acs.org/10.1021/acs.biomac.2c01016

Author Contributions

○C.E.W., M.K. and K.B.S.-D. contributed equally to this work. K.R. devised the idea for the manuscript. C.E.W., M.K., and K.B.S.-D. performed the experiments. All authors performed the analysis, wrote, and edited the manuscript. All authors have given approval to the final version of the manuscript.

Notes

The authors declare no competing financial interest.

ACKNOWLEDGMENTS

This work was supported by funding from NIBIB/NIH (R01EB017755-04), NIEHS/NIH (P30-ES002109), NSF (EF-2125118), the US Army Research Office under cooperative agreement W911NF-19-2-0026 for the Institute for Collaborative Biotechnologies, and the Army Research Office under Grant Number: W911NF-22-1-0185. C.E.W. thanks

https://doi.org/10.1021/acs.biomac.2c01016
Biomacromolecules 2023, 24, 628−639

NSERC (Canada) for a PGS-D award. K.B.S.-D. was supported by the National Institute of Environmental Health Sciences (T32-EW007020). C.M.W. and J.W. were also supported by the National Science Foundation Graduate Research Fellowship under Grant No. 1745302. The views and conclusions contained in this document are those of the authors and should not be interpreted as representing the official policies, either expressed or implied, of the Army Research Office or the U.S. Government. The U.S. Government is authorized to reproduce and distribute reprints for Government purposes notwithstanding any copyright notation herein.

REFERENCES

(1) Sellers, L. A.; Allen, A.; Morris, E. R.; Ross-Murphy, S. B. Mucus Glycoprotein Gels. Role of Glycoprotein Polymeric Structure and Carbohydrate Side-Chains in Gel-Formation. *Carbohydr. Res.* **1988**, *178*, 93−110.
(2) Nordgård, C. T.; Draget, K. I. Dynamic Responses in Small Intestinal Mucus: Relevance for the Maintenance of an Intact Barrier. *Eur. J. Pharm. Biopharm.* **2015**, *95*, 144−150.
(3) Argüeso, P.; Gipson, I. K. Epithelial Mucins of the Ocular Surface: Structure, Biosynthesis and Function. *Exp. Eye Res.* **2001**, *73*, 281−289.
(4) Bansil, R.; Turner, B. S. Mucin Structure, Aggregation, Physiological Functions and Biomedical Applications. *Curr. Opin. Colloid Interface Sci.* **2006**, *11*, 164−170.
(5) Duncan, G. A.; Jung, J.; Hanes, J.; Suk, J. S. The Mucus Barrier to Inhaled Gene Therapy. *Mol. Ther.* **2016**, *24*, 2043.
(6) Witten, J.; Ribbeck, K. The Particle in the Spider's Web: Transport through Biological Hydrogels. *Nanoscale* **2017**, *9*, 8080−8095.
(7) Witten, J.; Samad, T.; Ribbeck, K. Selective Permeability of Mucus Barriers. *Curr. Opin. Biotechnol.* **2018**, *52*, 124−133.
(8) Linden, S. K.; Sutton, P.; Karlsson, N. G.; Korolik, V.; McGuckin, M. A. Mucins in the Mucosal Barrier to Infection. *Mucosal Immunol.* **2008**, *1*, 183−197.
(9) Perez-Vilar, J.; Boucher, R. C. Reevaluating Gel-Forming Mucins' Roles in Cystic Fibrosis Lung Disease. *Free Radical Biol. Med.* **2004**, *37*, 1564−1577.
(10) Garland, A. L.; Walton, W. G.; Coakley, R. D.; Tan, C. D.; Gilmore, R. C.; Hobbs, C. A.; Tripathy, A.; Clunes, L. A.; Bencharit, S.; Stutts, M. J.; Betts, L.; Redinbo, M. R.; Tarran, R. Molecular Basis for PH-Dependent Mucosal Dehydration in Cystic Fibrosis Airways. *Proc. Natl. Acad. Sci. U.S.A.* **2013**, *110*, 15973−15978.
(11) Critchfield, A. S.; Yao, G.; Jaishankar, A.; Friedlander, R. S.; Lieleg, O.; Doyle, P. S.; Mckinley, G.; House, M.; Ribbeck, K. Cervical Mucus Properties Stratify Risk for Preterm Birth. *PLoS One* **2013**, *8*, No. e69528.
(12) Smith-Dupont, K. B.; Wagner, C. E.; Witten, J.; Conroy, K.; Rudoltz, H.; Pagidas, K.; Snegovskikh, V.; House, M.; Ribbeck, K. Probing the Potential of Mucus Permeability to Signify Preterm Birth Risk. *Sci. Rep.* **2017**, *7*, No. 10302.
(13) Cook, M. T.; Smith, S. L.; Khutoryanskiy, Vv. Novel Glycopolymer Hydrogels as Mucosa-Mimetic Materials to Reduce Animal Testing. *Chem. Commun.* **2015**, *51*, 14447−14450.
(14) Hall, D. J.; Khutoryanskaya, Ov.; Khutoryanskiy, Vv. Developing Synthetic Mucosa-Mimetic Hydrogels to Replace Animal Experimentation in Characterisation of Mucoadhesive Drug Delivery Systems. *Soft Matter* **2011**, *7*, 9620−9623.
(15) Hamed, R.; Fiegel, J. Synthetic Tracheal Mucus with Native Rheological and Surface Tension Properties. *J. Biomed. Mater. Res., Part A* **2014**, *102*, 1788−1798.
(16) Authimoolam, S. P.; Dziubla, T. D. Biopolymeric Mucin and Synthetic Polymer Analogs: Their Structure, Function and Role in Biomedical Applications. *Polymers* **2016**, *8*, 71.
(17) Kavanaugh, N. L.; Zhang, A. Q.; Nobile, C. J.; Johnson, A. D.; Ribbeck, K. Mucins Suppress Virulence Traits of Candida Albicans. *mBio* **2014**, *5*, No. e01911.
(18) Allen, A.; Pain, R. H.; Robson, T. R. Model for the Structure of the Gastric Mucous Gel. *Nature* **1976**, *264*, 88−89.
(19) Hattrup, C. L.; Gendler, S. J. Structure and Function of the Cell Surface (Tethered) Mucins. *Annu. Rev. Physiol.* **2008**, *70*, 431−457.
(20) Wagner, C. E.; Turner, B. S.; Rubinstein, M.; McKinley, G. H.; Ribbeck, K. A Rheological Study of the Association and Dynamics of MUC5AC Gels. *Biomacromolecules* **2017**, *18*, 3654−3664.
(21) Dekker, J.; Rossen, J. W. A.; Büller, H. A.; Einerhand, A. W. C. The MUC Family: An Obituary. *Trends Biochem. Sci.* **2002**, *27*, 126−131.
(22) Lieleg, O.; Vladescu, I.; Ribbeck, K. Characterization of Particle Translocation through Mucin Hydrogels. *Biophys. J.* **2010**, *98*, 1782−1789.
(23) Frenkel, E. S.; Ribbeck, K. Salivary Mucins Protect Surfaces from Colonization by Cariogenic Bacteria. *Appl. Environ. Microbiol.* **2015**, *81*, 332−338.
(24) Boegh, M.; Nielsen, H. M. Mucus as a Barrier to Drug Delivery - Understanding and Mimicking the Barrier Properties. *Basic Clin. Pharmacol. Toxicol.* **2015**, *116*, 179−186.
(25) Celli, J. P.; Turner, B. S.; Afdhal, N. H.; Keates, S.; Ghiran, I.; Kelly, C. P.; Ewoldt, R. H.; McKinley, G. H.; So, P.; Erramilli, S.; Bansil, R. Helicobacter Pylori Moves through Mucus by Reducing Mucin Viscoelasticity. *Proc. Natl. Acad. Sci. U.S.A.* **2009**, *106*, 14321−14326.
(26) Evans, D. F.; Pye, G.; Bramley, R.; Clark, A. G.; Dyson, T. J.; Hardcastle, J. D. Measurement of Gastrointestinal PH Profiles in Normal Ambulant Human Subjects. *Gut* **1988**, *29*, 1035−1041.
(27) Raynal, B. D. E.; Hardingham, T. E.; Thornton, D. J.; Sheehan, J. K. Concentrated Solutions of Salivary MUC5B Mucin Do Not Replicate the Gel-Forming Properties of Saliva. *Biochem. J.* **2002**, *362*, 289.
(28) Schipper, R. G.; Silletti, E.; Vingerhoeds, M. H. Saliva as Research Material: Biochemical, Physicochemical and Practical Aspects. *Arch. Oral. Biol.* **2007**, *52*, 1114−1135.
(29) Carlstedt, I.; Lindgren, H.; Sheehan, J. K.; Ulmsten, U.; Wingerup, L. Isolation and Characterization of Human Cervical-Mucus Glycoproteins. *Biochem. J.* **1983**, *211*, 13.
(30) Saltzman, W. M.; Radomsky, M. L.; Whaley, K. J.; Cone, R. A. Antibody Diffusion in Human Cervical Mucus. *Biophys. J.* **1994**, *66*, 508.
(31) Wang, Y. Y.; Lai, S. K.; Ensign, L. M.; Zhong, W.; Cone, R.; Hanes, J. The Microstructure and Bulk Rheology of Human Cervicovaginal Mucus Are Remarkably Resistant to Changes in PH. *Biomacromolecules* **2013**, *14*, 4429−4435.
(32) Crater, J. S.; Carrier, R. L. Barrier Properties of Gastrointestinal Mucus to Nanoparticle Transport. *Macromol. Biosci.* **2010**, *10*, 1473−1483.
(33) Hill, D. B.; Vasquez, P. A.; Mellnik, J.; McKinley, S. A.; Vose, A.; Mu, F.; Henderson, A. G.; Donaldson, S. H.; Alexis, N. E.; Boucher, R. C.; Forest, M. G. A Biophysical Basis for Mucus Solids Concentration as a Candidate Biomarker for Airways Disease. *PLoS One* **2014**, *9*, No. e87681.
(34) Pelletier, V.; Kilfoil, M.*Software Research Tools*; Kilfoil Lab, 2007.
(35) Crocker, J. C.; Weeks, E. R.Particle Tracking Using IDL. http://www.physics.emory.edu/faculty/weeks//idl/ (accessed Jan 01, 2018).
(36) Metzler, R.; Jeon, J. H.; Cherstvy, A. G.; Barkai, E. Anomalous Diffusion Models and Their Properties: Non-Stationarity, Non-Ergodicity, and Ageing at the Centenary of Single Particle Tracking. *Phys. Chem. Chem. Phys.* **2014**, *16*, 24128−24164.
(37) Metzler, R.; Klafter, J. The Random Walk's Guide to Anomalous Diffusion: A Fractional Dynamics Approach. *Phys. Rep.* **2000**, *339*, 1−77.
(38) Evers, F.; Zunke, C.; Hanes, R. D. L.; Bewerunge, J.; Ladadwa, I.; Heuer, A.; Egelhaaf, S. U. Particle Dynamics in Two-Dimensional

Random Energy Landscapes - Experiments and Simulations. *Phys. Rev. E: Stat., Nonlinear, Soft Matter Phys.* **2013**, *88*, No. 022115.
(39) Li, L.; Lieleg, O.; Jang, S.; Ribbeck, K.; Han, J. A Microfluidic in Vitro System for the Quantitative Study of the Stomach Mucus Barrier Function. *Lab Chip* **2012**, *12*, 4071−4079.
(40) Li, L. D.; Crouzier, T.; Sarkar, A.; Dunphy, L.; Han, J.; Ribbeck, K. Spatial Configuration and Composition of Charge Modulates Transport into a Mucin Hydrogel Barrier. *Biophys. J.* **2013**, *105*, 1357−1365.
(41) Jaishankar, A.; McKinley, G. H. A Fractional K-BKZ Constitutive Formulation for Describing the Nonlinear Rheology of Multiscale Complex Fluids. *J. Rheol.* **2014**, *58*, 1751.
(42) von Diezmann, L.; Shechtman, Y.; Moerner, W. E. Three-Dimensional Localization of Single Molecules for Super-Resolution Imaging and Single-Particle Tracking. *Chem. Rev.* **2017**, *117*, 7244−7275.
(43) Wagner, C. E.; Wheeler, K. M.; Ribbeck, K. Mucins and Their Role in Shaping the Functions of Mucus Barriers. *Annu. Rev. Cell Dev. Biol.* **2018**, *34*, 189−215.
(44) Caldara, M.; Friedlander, R. S.; Kavanaugh, N. L.; Aizenberg, J.; Foster, K. R.; Ribbeck, K. Mucin Biopolymers Prevent Bacterial Aggregation by Retaining Cells in the Free-Swimming State. *Curr. Biol.* **2012**, *22*, 2325−2330.
(45) Meldrum, O. W.; Yakubov, G. E.; Bonilla, M. R.; Deshmukh, O.; McGuckin, M. A.; Gidley, M. J. Mucin Gel Assembly Is Controlled by a Collective Action of Non-Mucin Proteins, Disulfide Bridges, Ca2+-Mediated Links, and Hydrogen Bonding. *Sci. Rep.* **2018**, *8*, No. 5802.
(46) Raynal, B. D. E.; Hardingham, T. E.; Sheehan, J. K.; Thornton, D. J. Calcium-Dependent Protein Interactions in MUC5B Provide Reversible Cross-Links in Salivary Mucus*. *J. Biol. Chem.* **2003**, *278*, 28703−28710.
(47) Bansil, R.; Celli, J. P.; Hardcastle, J. M.; Turner, B. S. The Influence of Mucus Microstructure and Rheology in Helicobacter Pylori Infection. *Front. Immunol.* **2013**, *4*, 310.
(48) Larhed, A. W.; Artursson, P.; Gråsjö, J.; Björk, E. Diffusion of Drugs in Native and Purified Gastrointestinal Mucus. *J. Pharm. Sci.* **1997**, *86*, 660−665.
(49) Ewoldt, R. H.; Johnston, M. T.; Caretta, L. M.Experimental Challenges of Shear Rheology: How to Avoid Bad Data. In *Complex Fluids in Biological Systems. Biological and Medical Physics*; Spagnolie, S., Ed.; Biomedical Engineering Springer: New York, NY, 2015; pp 207−241 DOI: 10.1007/978-1-4939-2065-5_6.
(50) Song, J.; Winkeljann, B.; Lieleg, O. The Lubricity of Mucin Solutions Is Robust toward Changes in Physiological Conditions. *ACS Appl. Bio. Mater.* **2019**, *2*, 3448−3457.
(51) Radicioni, G.; Cao, R.; Carpenter, J.; Ford, A. A.; Wang, T. T.; Li, Y.; Kesimer, M. The Innate Immune Properties of Airway Mucosal Surfaces Are Regulated by Dynamic Interactions between Mucins and Interacting Proteins: The Mucin Interactome. *Mucosal Immunol.* **2016**, *9*, 1442−1454.
(52) Larhed, A. W.; Artursson, P.; Björk, E. The Influence of Intestinal Mucus Components on the Diffusion of Drugs. *Pharm. Res.* **1998**, *15*, 66−71.

https://doi.org/10.1021/acs.biomac.2c01016
Biomacromolecules 2023, 24, 628−639